Original Article

The pannexin-1 channel regulates pyroptosis through autophagy in a mouse model of sepsis-associated encephalopathy

Yupeng Lei[1,2#], Ruixi Zhou[1,2#], Xuemei Sun[1,2], Fajuan Tang[1,2], Hu Gao[1,2], Lin Chen[1,2], Xihong Li[1,2]

[1]Department of Pediatrics, West China Second University Hospital, Sichuan University, Chengdu, China; [2]Key Laboratory of Birth Defects and Related Diseases of Women and Children (Sichuan University), Ministry of Education, Chengdu, China

Contributions: (I) Conception and design: Y Lei, X Li; (II) Administrative support: X Li; (III) Provision of study materials or patients: R Zhou, X Sun, F Tang; (IV) Collection and assembly of data: X Li, H Gao, L Chen; (V) Data analysis and interpretation: Y Lei, R Zhou, X Li; (VI) Manuscript writing: All authors; (VII) Final approval of manuscript: All authors.

[#]These authors contributed equally to this work.

Correspondence to: Xihong Li. Department of Pediatrics, West China Second University Hospital, Sichuan University, Chengdu 610041, China. Email: lixihonghxey@163.com.

Background: Sepsis-associated encephalopathy (SAE) is a diffuse brain dysfunction caused by sepsis. Pyroptosis and autophagy are important mechanisms in the pathogenesis of sepsis, and also pannexin-1 is involved in the occurrence of sepsis. However, role of pannexin-1 in SAE and its relationship with pyroptosis and autophagy are unclear. This study examined the relationship between pannexin-1 and pyroptosis, and further explore the relationship between pyroptosis and autophagy in SAE mice.

Methods: A SAE mouse model was established by cecal ligation and puncture (CLP). Different groups of mice were administrated probenecid (PRB), 3-methyladenine (3-MA), or a vehicle control and the survival rates were monitored at different time points. Cortical pathological changes were examined by hematoxylin and eosin (HE) staining. The expression of cortical pannexin-1 and adenosine monophosphate-activated protein kinase (AMPK), as well as pyroptosis and autophagy related proteins, was detected by Western blotting and immunofluorescence analysis. The ultrastructure of neurons was observed by transmission electron microscopy.

Results: Septic mice showed significantly higher rates of mortality and cortical pathological change compared to control mice. In addition, the pannexin-1 and AMPK signaling pathway were activated in the cerebral cortex of the septic mice, coupled with the activation of pyroptosis and incomplete activation of autophagy. Inhibition of pannexin-1 expression reduce the rates of mortality and the cortical pathological changes in the mice, further activated the AMPK signaling pathway, inhibited pyroptosis, and completely activated autophagy. The inhibition of autophagy may cause pyroptosis to reactivate.

Conclusions: The present findings suggested that in SAE mice, pannexin-1 may regulate neuronal pyroptosis through autophagy. Moreover, the regulation of autophagy may be related to the AMPK signaling pathway. Inhibiting pannexin-1 expression in SAE mice may have a neuroprotective effect.

Keywords: Sepsis associated encephalopathy; pannexin-1; autophagy; pyroptosis; adenosine monophosphate-activated protein kinase signaling pathway (AMPK signaling pathway)

Submitted Nov 19, 2021. Accepted for publication Dec 17, 2021.

doi: 10.21037/atm-21-6579

View this article at: https://dx.doi.org/10.21037/atm-21-6579

Introduction

Sepsis is a global public health problem that is associated with an extremely high rate of morbidity and mortality (1,2). Sepsis is a systemic inflammatory reaction syndrome that causes a dysregulated host response to infections (3,4), leading to multiple organ impairment and dysfunction. The pathogenesis of sepsis is related to the sophisticated interaction between the host and the pathogens (5). Sepsis-associated encephalopathy (SAE) is a diffuse brain disorder caused by sepsis (6), clinically manifesting as a series of brain disorders, such as lethargy, delirium, and comas (7,8). Early detection and treatment of SAE is paramount to patient prognosis (9).

Autophagy, apoptosis and pyroptosis are common ways of cell death, they also differ in the mechanism. Apoptosis is a highly regulated form of cell death, is essential for our homeostasis and pathological process, Apoptosis is characterised by some characteristic morphological changes in the cell, as well as a number of enzyme-dependent biochemical processes that result in the removal of cells from the body with minimal damage to surrounding tissues (10). Pyroptosis is defined as a programmed process of cell death which is related to inflammation (11,12). Pyroptosis can promote the process of inflammation. Pyroptotic bodies, similar to apoptotic bodies, can affect cells which play an essential role in pyroptosis by affecting chromatin damage and pyknosis (13). A large number of non-selective pores distributed on the cell membrane can cause the loss of cell membrane integrity and the release of intracellular inflammatory factors (such as interleukin 1β and tumor necrosis factor α), thereby triggering an inflammatory response (14). Autophagy, as one of the modes of programmed cell death, is a conserved cellular self-regulation mechanism (15). Autophagosomes are formed by phagocytosis and combine with lysosomes under the influence of various stressors. Autophagy recognizes a variety of inflammation-related substances to regulate the inflammatory response (16). Pyroptosis and autophagy are two common cell death modes in sepsis. In recent study, they have found the pannexin-1 involved in the cell death pathway of apoptosis, however, aims of our study try to elaborate whether pannexin-1 involved in pyroptosis and autophagy.

Pannexin-1 is a non-selective ion-gated channel protein that regulates the release of various nucleotides and adenosine triphosphate (ATP) (17). When pannexin-1 is stimulated to open, it induces ATP outflow, which further activates inflammasomes and induces pyroptosis (18). Probenecid (PRB) has been used in the clinical treatment of hyperuricemia and may delay the excretion of penicillin (19). A recent study demonstrated that PRB can inhibit the opening of pannexin-1, thereby inhibiting the inflammatory response and further inhibiting pyroptosis (20,21). However, it remains unclear whether the inhibition of pannexin-1 can reduce the risk of SAE by inhibiting pyroptosis. Furthermore, the relationship between pyroptosis and autophagy in SAE remains unclear. As a specific inhibitor of autophagy, 3-methyladenine (3-MA) can effectively block the formation of autophagosomes and autophagy (22), and is a good agent for exploring the connection between pyroptosis and autophagy in SAE.

The adenosine monophosphate-activated protein kinase (AMPK) is a conservative intracellular energy sensor. Previous studies have shown that AMPK is a necessary kinase for autophagy (23) and it regulates autophagy by phosphorylating beclin-1 (BECN1) at threonine 388 to form phosphorylated AMPK (p-AMPK) (24). Previous studies have shown that the expression levels of caspase-1, caspase-11, apoptosis-associated speck-like protein (ASC), and absent in melanoma 2 (AIM2) increase when pyroptosis occurs in the cerebral cortex of mice (25,26). Therefore, the presence of these proteins may be indicative of pyroptosis. During autophagy, microtubule-associated protein light chain 3 (LC3-I) is coupled with phosphatidylethanolamine to form LC3-II, recruiting the autophagy membrane (27). SQSTM1/p62 is associated with the degradation of misfolded proteins, damaged or excess organelles, intracellular bacterial and viral capsids, and various signal proteins or complexes in autophagy (28,29). Therefore, LC3 and SQSTM1/p62 may be useful markers of autophagy.

This study examined the relationship between pannexin-1 and pyroptosis, and further explore the relationship between pyroptosis and autophagy in SAE mice. PRB was used to inhibit pannexin-1 and the effects on pyroptosis in the cerebral cortex of mice was observed. Furthermore, 3-MA was used to inhibit autophagy to further examine the relationship between pyroptosis and autophagy.

We present the following article in accordance with the ARRIVE reporting checklist (available at https://dx.doi.org/10.21037/atm-21-6579).

Methods

Animals

All animal experiments were approved by the Research

Animal Care Committee of the Sichuan University (Sichuan, China) [No. (2021) Animal Ethics Approval No. 046], in compliance with Sichuan University guidelines for the care and use of animals. A protocol was prepared before the study without registration. Healthy and clean male specific pathogen free (SPF) C57BL/6 mice (13–16 g, 30 days old), were purchased from the Sichuan Jianyang Dashuo Animal Science and Technology Co., Ltd. (Shu ICP 09003144). The mice were housed in a humidified environment (55–58%) with controlled temperature (22–25 ℃) and a 12-h light/dark cycle, and given free access to water and food.

Mouse model of sepsis and experimental groups

The *in vivo* mouse sepsis model was constructed by cecal ligation and puncture (CLP), as previously described (30). Chloral hydrate [10% (w/v), 3 mL/kg] was intraperitoneally administered to induce deep anesthesia in the mice. After shaving and disinfecting the abdominal area, an incision along the middle line of the abdomen was created. An 18-gauge hollow-bore needle was used to puncture the cecum after it was isolated and ligated. The cecum was placed back to the abdominal cavity after extruding the feces. A layer-by-layer suture was made to close the wound. Saline [0.9% (w/v), 50 mL/kg] was administered to the mice to compensate for blood loss during the operation. The same procedure was performed in the mice in the sham-operated group, but without ligation, puncture, or other treatments.

Drug administration

Experimental animals were assigned into the following groups via computer-based randomization: sham, CLP, CLP + vehicle (Veh), CLP + PRB, and CLP + PRB + 3-MA. The PRB (Sigma-Aldrich, St. Louis, MO) injection solution (pH 7.3) was dissolved in NaCl solution (0.9%), supplemented with NaOH (0.1 M), Tris (0.1 M), and HCl (2 M) for pH adjustment. PRB (50 mg/kg) was administered to mice in the CLP + PRB and CLP + PRB + 3-MA groups via intraperitoneal injection after CLP surgery. The doses of PRB treatment were based on previous literatures (31,32). Mice in the CLP + Veh group received equal volumes of the solvent solution at the same time points during the CLP procedure. Furthermore, mice in the CLP + PRB + 3-MA group received an intracerebroventricular injection of 3-MA (5142-23-4, Selleck, Texas, USA) (0.5 mg/kg) in the left lateral ventricle (2.4 mm ventral, 0.2 mm posterior, and 0.9 mm lateral to the bregma) following CLP surgery, The doses of 3-MA treatment were based on previous literatures (33,34).

Histological examination

For cardiac perfusion, paraformaldehyde (PFA, 4% w/v, 100 mL) and saline (0.9% w/v, 100 mL) was injected into the left ventricle of the mice under anesthesia. Brain tissue was obtained and fixed with PFA for 48 hours at 4 ℃. The fixed tissue was dissected on the coronal plane from the optic chiasm to the posterior end (length: 1 cm) and embedded in paraffin. Sections of the brain tissue (6 μm) were stained with hematoxylin and eosin (HE). Slides were visualized using the Leica inverted optical microscope (Leica, Mannheim, Germany) and images were captured.

Western blotting

The brain tissue was collected under anesthesia and the cortical tissue was dissected in ice-cold lysis buffer [10 mg/L NP-40; 150 mmol/L NaCl; 50 mmol/L Tris-HCl, pH 7.4; 0.1% (v/v) protease inhibitor cocktail (Roche, Basel, Switzerland)] for 30 minutes at 4 ℃. After homogenization on ice and centrifugation (4 ℃, 14,000 g, 30 minutes), protein loading buffer was added to the supernatant (Beyotime, Shanghai, China) and the samples were denaturation at 100 ℃. The protein content was determined using the BCA Analysis Kit (Beyotime). Equal amounts of protein were separated using sodium dodecyl-sulfate polyacrylamide gel electrophoresis and transferred onto methanol-treated polyvinylidene difluoride membranes (Millipore, Billerica, MA, USA). Membranes were blocked for 1 hour at room temperature using 5% skim milk (w/v) in Tris-buffered saline supplemented with Tween 20 (TBS-T). The membranes were then incubated with the following primary antibodies at 4 ℃ overnight: AMPK (1:1,000, ab32047, Abcam, Cambridge, UK), p-AMPK (1:1,000, ab133448, Abcam), the biomarker of proptosis includes pannexin-1 (D9M1C) rabbit mAb (1:1,000, 91137s, CST, Beverly, MA, USA), ASC/TMS1 (D2W8U) rabbit mAb (1:1,000, 67824, CST), AIM2 antibody (mouse-specific) (1:1,000, 63660, CST), caspase-1 (1:1,000, ab207802, Abcam), and caspase-11 (1:1,000, ab180673, Abcam). the biomarker of autophagy includes anti-LC3B antibody (1:1,000, ab48394, Abcam), anti-SQSTM1/p62 antibody (1:1,000, ab56416, Abcam). Membranes were

then washed 3 times with TBS-T followed by incubation with the secondary antibodies [including HRP-conjugated anti-rabbit (1:5,000, ZSGB-BIO) and HRP-conjugated anti-mouse (1:5,000, ZSGB-BIO)] for 1 hour at room temperature. After washing the membranes in TBS-T 3 times, enhanced chemiluminescence (Millipore) was used to visualize the protein bands. The gel imaging analysis system (Bio-Rad, Hercules, CA, USA) was used to acquire images within the linear range. The Image J Analyzer Software (NIH, Bethesda, MD, USA) was used to quantitatively analyzing the relative intensity of the bands. Glyceraldehyde 3-phosphate dehydrogenase (GAPDH) was used as an internal control in this study.

Immunofluorescence staining

After cardiac perfusion (as mentioned in 2.4), the whole brain was immediately collected and dissected. The optic chiasma, coronal plane, and an additional 1 cm of tissue were fixed at 4 ℃ overnight in 4% (w/v) PFA. Agarose (2.5% w/v) was used to fix the tissue before 40 μm sections were prepared under the oscillating microtome (Leica). After washing in phosphate-buffered saline (PBS) 3 times, the sections were blocked for 30 minutes in Triton X (0.3% v/v), followed by incubation for 1 hour in a mixed solution containing bovine serum albumin (3% w/v, ST023, Beyotime), fresh bovine serum (2% v/v), and Triton X-100 (0.2% v/v) at room temperature. The sections were incubated with the following primary antibodies at 4 ℃ overnight: ASC/TMS1 (D2W8U) rabbit mAb (1:200), anti-LC3B antibody (1:500), or anti-NeuN (neuron specific nuclear) mouse monoclonal antibody (ab104224, 1:500, Abcam). The sections were then washed 3 times in PBS, followed by incubation with secondary antibodies for 2 hours at room temperature in the dark. The secondary antibodies used were Cy3-conjugated anti-mouse IgG (715–165-151, 1:800, Jackson Immuno-Research, USA), DyLight 488-conjugated anti-rabbit IgG (ab96899, 1:500, Abcam), and DyLight 488-conjugated anti-goat IgG (ab150129, 1:500, Abcam). Nuclear DNA staining was performed by incubation with 4,6-diamidino-2-phenylindole (DAPI, C1002, 1:500, Beyotime) for 10 minutes in the dark at room temperature. The sections were then placed on slides using an anti-fluorescence quenching agent (Beyotime). Sections were observed using the confocal laser scanning microscope (Olympus, Tokyo, Japan) using proper laser beams and filters [DyLight 488 (excitation peak 493 nm, emission peak 518 nm) or Cy3 (excitation peak 550 nm, emission peak 570 nm)]. The FV10-ASW-4.2 software (Olympus) was used to acquire digital images.

Transmission electron microscopy (TEM)

Cortical tissue (1 mm^3) was sliced after fixation, washed in PBS, and fixed using osmium tetroxide (1%) and glutaraldehyde (3%) for 2 hours. Epoxy resin was used to embed the tissue before 0.12 μm sections were prepared. The sections were then stained by lead citrate (0.2%) and uranium acetate (1%). Sections were analyzed using the HT7700 120KV TEM (Hitachi, Tokyo, Japan).

Statistical analysis

Survival rates were analyzed using the Kaplan-Meier method. The values used in the experimental results were presented as average value ± standard error of the mean (SEM). The SPSS version 19.0 software (SPSS, Inc., Chicago, IL, USA) was used for statistical analyses. The Student-Newman-Keuls post-hoc test and one-way analysis of variance were used for examining the differences between groups. P values <0.05 were considered statistically significant.

Results

Survival rate analysis

In the sham group, all mice (30/30, 100%) survived at all time points examined (*Figure 1*). In the CLP group, the 12 hours survival rate was significantly lower (10/30, 33.33%), and the 24 hours survival rate was further decreased (4/30, 13.33%). There was no significant difference in the survival rates between mice in the CLP + Veh group (9/30, 30.00%) and mice in the CLP group (4/30, 13.33%). Compared with mice in the CLP and CLP + Veh groups, the survival rate of mice in the CLP + PRB group was increased, with 12 and 24 hours survival rates of 46.67% (14/30) and 23.33% (7/30), respectively. The survival rate of mice in the CLP + PRB + 3-MA group (1/30, 3.33%) was significantly lower than that of the CLP + PRB group (5/30, 16.67%).

Mice that had undergone CLP showed obvious pathological changes, with activation of the pannexin-1 and AMPK signaling pathway

Compared with the sham-operated mice, the cortex of

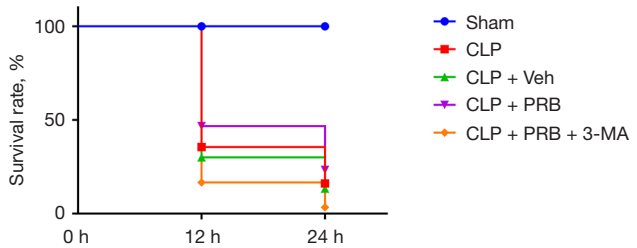

Figure 1 The survival rate of mice at different time points (n=30). Data are shown as the mean ± SEM obtained from three independent experiments. CLP, cecal ligation and perforation; Veh, vehicle; PRB, probenecid; 3-MA, 3-methyladenine; SEM, standard error of mean.

the CLP mice showed loosening and edema, disordered cell arrangement, shrinkage of cells, pyknosis of nuclei, and significant widening of the space around the cells (arrows) (*Figure 2A*). Concurrently, the levels of pannexin-1 expression and the ratio of p-AMPK/AMPK in the cortex of the CLP group were higher at both 12 and 24 hours compared to those observed in the cortex of the sham group (*Figure 2B,2C*).

Pyroptosis and autophagy were activated in mice that had undergone CLP

The expression levels of pyroptosis-related proteins were compared between sham mice and CLP mice. At 12 hours, the levels of caspase-1, caspase-11, ASC, and AIM2 expression in the CLP mice were remarkably elevated compared to the sham-operated mice (*Figure 3A*). Immunofluorescence staining in the mouse cortex demonstrated that ASC expression was higher in the CLP mice compared to the sham-operated mice. Co-staining the astrocytes and microglia alongside the neurons revealed that ASC was mainly expressed in the neurons, followed by the microglia and astrocytes (*Figure 3B*). The ratio of LC3-II/I expression in the cortex of the CLP mice was higher than that in the cortex of the sham mice. However, the level of SQSTM1/p62 expression was similar between the groups (*Figure 3C*). Immunofluorescence staining showed that the LC3 fluorescence signal observed in the cortex of the CLP mice was enhanced compared to the sham-operated group. In addition, the expression of LC3 was most pronounced in the neurons, followed by that in the microglia and astrocytes (*Figure 3D*). TEM revealed that the cortical neurons of sham mice were not significantly damaged and that the organelles were intact. In contrast, autophagosomes were observed in the neurons of CLP mice and there was a large number of damaged proteins and organelle fragments that had not been degraded (*Figure 3E*).

Intervention with PRB improved the pathology in the cortex of CLP mice, and decreased the expression of pannexin-1 and activated the expression of AMPK

The cortical tissue from mice in the CLP and CLP + Veh groups showed loosening and edema, disordered arrangement of cells, shrinkage of cells, pyknosis of nuclei, and obvious widening of the space around the cells (arrows) (*Figure 4A*). Treatment of CLP mice with PRB (CLP + PRB group) reduced the extent of the pathological changes in the cortex compared to that observed in the CLP and CLP + Veh groups (*Figure 4A*). Western blot analysis showed that the level of pannexin-1 expression in the CLP + PRB group was significantly lower, while the ratio of p-AMPK/AMPK was higher than those in the CLP and CLP + Veh groups (*Figure 4B,4C*).

PRB alleviates pyroptosis and activates autophagy in CLP mice

The levels of caspase-1, caspase-11, ASC, and AIM2 expression in the cortex of CLP mice after PRB intervention were lower than those in the CLP and CLP + Veh groups (*Figure 5A*). Immunofluorescence staining revealed that the ASC fluorescence signal in the cortex of CLP mice was significantly reduced after intervention with PRB (*Figure 5B*). In addition, PRB increased the LC3-II/I ratio and decreased the SQSTM1/p62 expression levels compared to CLP mice and CLP + Veh mice (*Figure 5C*). Furthermore, the fluorescence signal of LC3 was also significantly enhanced after PRB administration compared to CLP mice without PRB treatment (*Figure 5D*). TEM observation of the cortical neurons in the CLP + PRB group revealed that the organelle structure was generally normal and the substances in the autophagosomes were effectively degraded, forming multiple autophagy vesicles (*Figure 5E*).

3-MA inhibits neuron autophagy and activates pyroptosis

To further examine the relationship between autophagy and pyroptosis, the autophagy inhibitor 3-MA was administered to the CLP mice. CLP mice given both PRB and 3-MA (CLP + PRB + 3-MA group) showed elevated expression

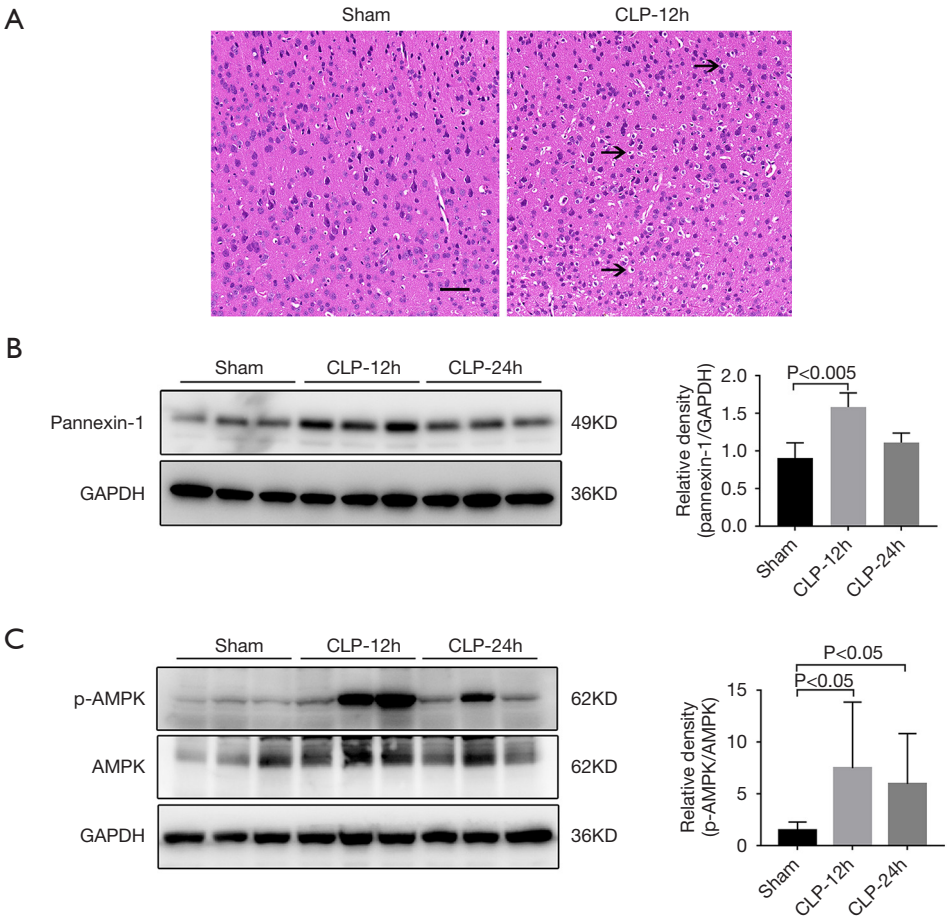

Figure 2 Sepsis associated encephalopathy was successfully established in mice by CLP. (A) Cerebral tissues were stained by HE in the sham mice and CLP mice to observe the pathological changes in the cortex of the mice 12 hours after surgery. Loosening and edema, disordered cell arrangement, shrinkage of cells, pyknosis of nuclei, and significant widening of the space around the cells were indicated by arrows. Scale bar =50 μm. (B) Pannexin-1 and p-AMPK/AMPK protein expression were elevated in the cortex of the CLP group at 12 and 24 hours. GAPDH was used as internal reference for normalization and the results were shown as relative protein levels. The histogram shows the relative expression of pannexin-1. (C) p-AMPK/AMPK protein expression were elevated in the cortex of the CLP group at 12 and 24 hours. The histogram shows the relative expression of p-AMPK/AMPK. Data are expressed as the mean ± SD (n=6 per group). SAE, sepsis associated encephalopathy; CLP, cecal ligation and perforation; AMPK, adenosine monophosphate-activated protein kinase; SD, standard deviation.

of caspase-1, caspase-11, ASC, and AIM2 expression compared to mice in the CLP + PRB group (*Figure 6A*), and the fluorescence signal of ASC was further enhanced (*Figure 6B*). In the cortex of mice in CLP + PRB + 3-MA group, the LC3-II/I ratio was decreased and the SQSTM1/p62 expression level was increased compared to mice in the CLP + PRB group (*Figure 6C*), and the fluorescence signal of LC3 was decreased (*Figure 6D*). TEM observations revealed no autophagosome formation in the cortical neurons of the CLP + PRB + 3-MA group. However, obvious mitochondrial swelling and mitochondrial crest rupture were observed in this latter group (*Figure 6E*).

Discussion

This study demonstrated significantly higher mortality rates in mice subjected to CLP compared to sham-operated mice, indicating that the sepsis model was well-established, as previously described (30). In addition, pathological changes were observed in the cortex of

the mice after CLP treatment, while no changes were observed in the sham operation group, indicating that the septic model established by CLP could lead to cortical injury and SAE (35).

Pannexin-1 is a non-selective ion-gated channel protein that regulates the release of various nucleotides and adenosine triphosphate (ATP) (17). When pannexin-1 is stimulated to open, it induces ATP outflow, which further activates inflammasomes and induces pyroptosis (18). The opening of the pannexin-1 channel may activate NLRP3, ASC, and caspase-1, among others, leading to pyroptosis (36,37). The AMPK is a conservative intracellular energy sensor and has been shown to be a necessary kinase for autophagy (23). In our SAE mouse model, the levels of pannexin-1 and the ratio of p-AMPK/AMPK in the cortex of the mice were elevated, suggesting that both pathways were concurrently activated in SAE. Furthermore, caspase-1 and caspase-11 are believed to mediate the activity of canonical and non-canonical pathways of pyroptosis, respectively (38). In the process of pyroptosis, a variety of inflammasomes are formed, such as AIM2/ASC and NLRP3/ASC (37). These inflammasomes further promote the maturation of inflammatory factors and eventually lead to the occurrence of pyroptosis (12). In our study, the levels of caspase-1, caspase-11, ASC, and AIM2 expression in the cortex of SAE mice were increased, indicating that pyroptosis occurred at the same time as SAE. LC3 and SQSTM1/p62 are indispensable components in autophagy (39,40). Studies have shown that during autophagy, LC3-I in the cytoplasm is coupled with phosphatidylethanolamine to form LC3-II, which then recruits the autophagy membrane, suggesting that LC3-II is a protein related to autophagy membrane specificity (27). Meanwhile, SQSTM1/p62 is associated with the degradation of misfolded proteins, damaged or excess organelles, intracellular bacterial and viral capsids, and various signal proteins or complexes in autophagy (28,29). In addition, SQSTM1/p62 is swallowed by autophagosomes and eventually degraded in autophagy by combining with these compounds (27). Therefore, LC3 and SQSTM1/p62 may be used as markers of autophagy. In this current study, TEM demonstrated that autophagosomes were present in the cortical region of the SAE mice, and undegraded organelles and protein fragments were observed in autophagy. Furthermore, Western blot analysis

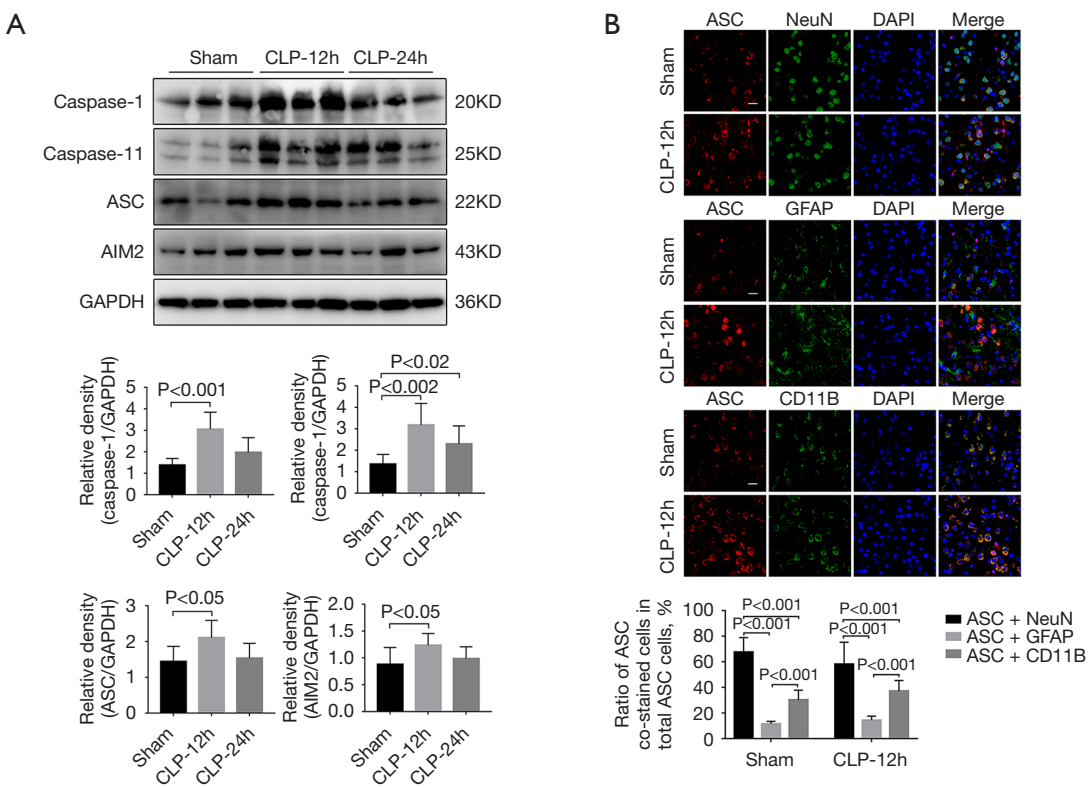

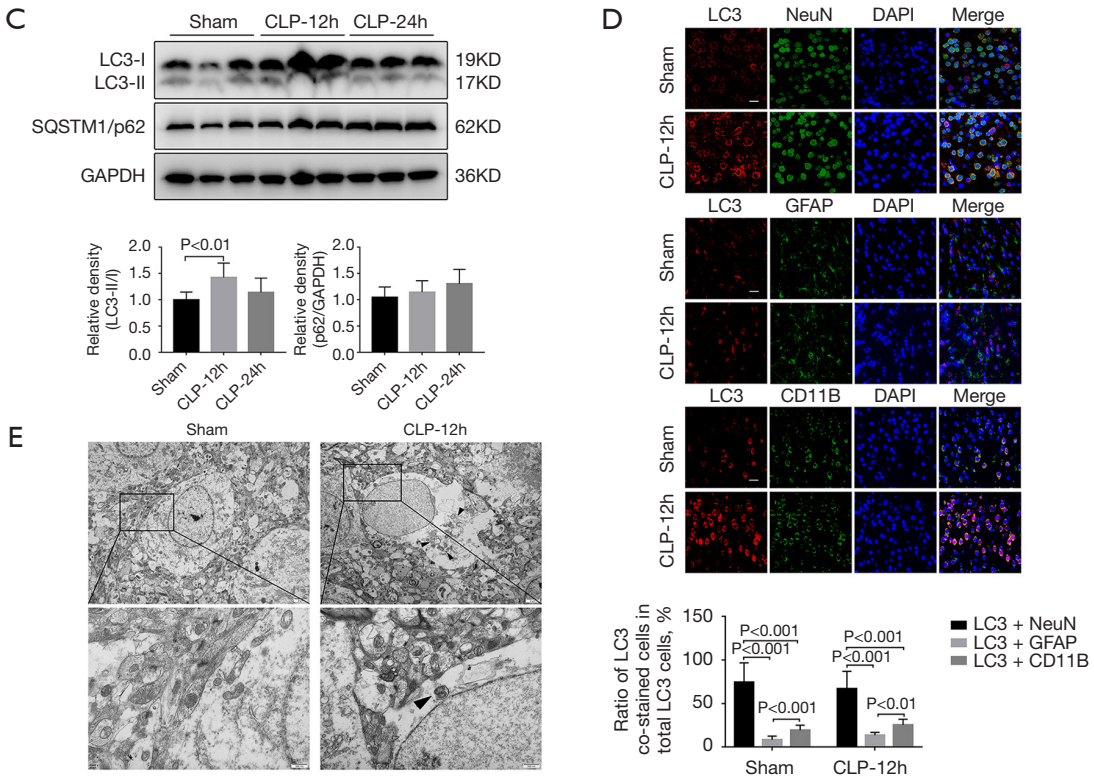

Figure 3 Pyroptosis and autophagy were activated in SAE mice induced by CLP. (A) Expression levels of caspase-1, caspase-11, ASC, and AIM2 were detected by Western blotting. GAPDH was used as internal reference for normalization and the results are shown as relative protein levels in the histograms. (B) Fluorescence intensity of ASC (red) and NeuN/GFAP/CD11B (green) were detected by immunofluorescence staining (12 hours after surgery). The rate of co-localization of ASC with NeuN, GFAP, and CD11B are shown in the histogram. Scale bar =20 μm. Data are expressed as the mean ± SD (n=6 per group). (C) Expression levels of LC3-II/I and p62 were detected by Western blotting. GAPDH was used as an internal reference for normalization and the results are shown as relative protein levels in the histograms. (D) Fluorescence intensities of LC3 (red) and NeuN/GFAP/CD11B (green) were detected by immunofluorescence staining (12 hours after surgery). Co-localization of LC3 with NeuN, GFAP, and CD11B is shown in the histogram. Scale bar =20 μm. (E) At 12 hours post-surgery, the ultrastructure of the cortical neurons in the sham and CLP groups was observed by TEM. Morphology was normal in the sham group. The CLP group showed autophagosomes in the neurons, which contained a large number of damaged proteins and organelle fragments that had not been degraded. Scale bar =1 and 2 μm. Data are expressed as the mean ± SD (n=6 per group). SAE, sepsis associated encephalopathy; CLP, cecal ligation and perforation; ASC, apoptosis-associated speck-like protein; AIM2, absent in melanoma 2; GAPDH, glyceraldehyde 3-phosphate dehydrogenase; NeuN, neuron specific nuclear; GFAP, glial fibrillary acidic protein; TEM, transmission electron microscope; SD, standard deviation.

demonstrated that the LC3-II/I ratio in the cortex was elevated, suggesting the formation of autophagy. However, the levels of SQSTM1/p62 expression in the cortex tissue of the sham-operated and CLP mice were similar because SQSTM1/p62 mediated the transfer of damaged organelles and protein fragments to autophagosomes, where they were not effectively degraded (41). Overall, these findings suggested that pyroptosis and autophagy occurred in mice after CLP.

Pyroptosis is a type of inflammation-related programmed cell death which leads to the release of inflammatory factors and triggers topical inflammation (38). Inhibition of pyroptosis for the treatment of sepsis has recently become a research focus. Pannexin-1 has been shown to play an important role in the occurrence of pyroptosis and this current study demonstrated that the inhibition of pannexin-1 may inhibit pyroptosis, and thus alleviate SAE, providing a novel therapeutic target for

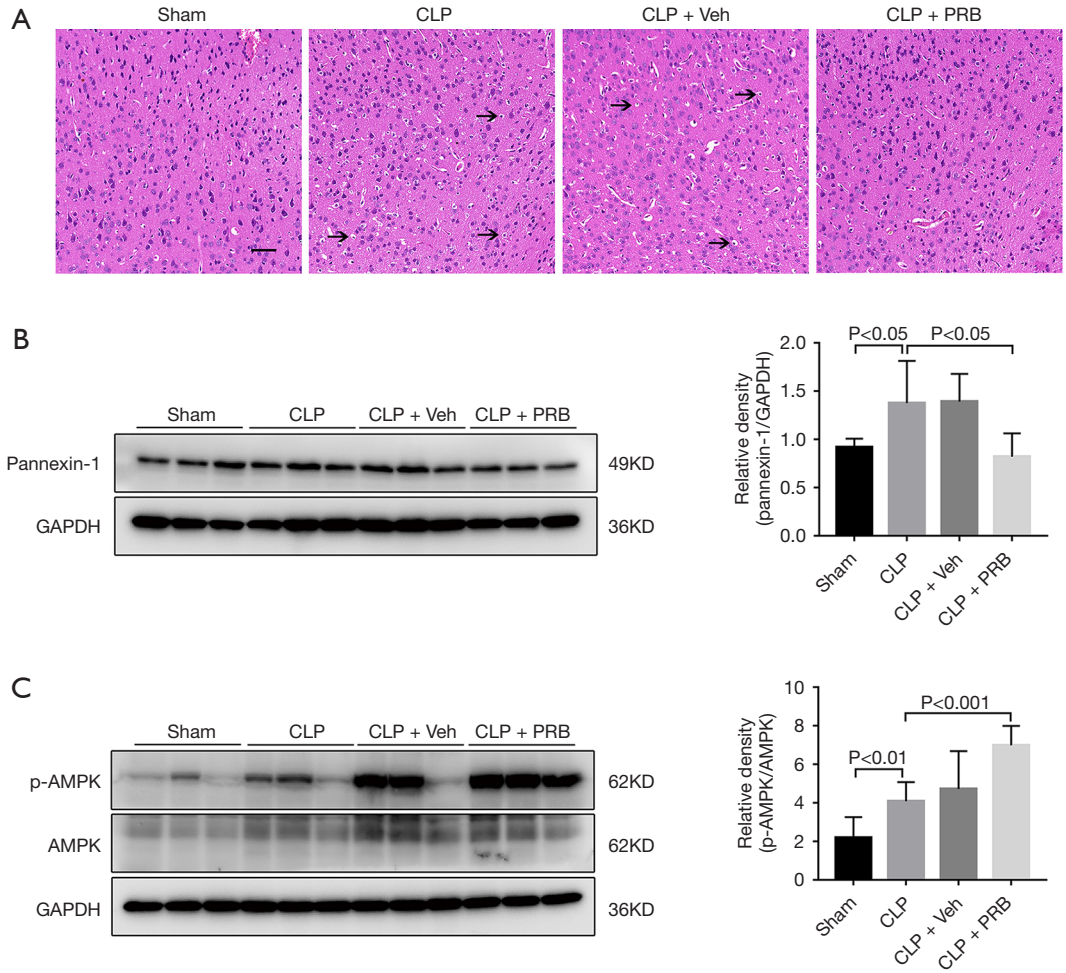

Figure 4 Pyroptosis was alleviated in SAE mice after treatment with PRB. (A) HE staining of the cerebral tissues show the pathological changes in the cortex of the mice. loosening and edema, disordered arrangement of cells, shrinkage of cells, pyknosis of nuclei, and obvious widening of the space around the cells were indicated by arrows. Scale bar =50 μm. (B,C) The expression of pannexin-1 and p-AMPK/AMPK were detected by Western blotting. GAPDH was used as internal reference for normalization and the results are shown as relative protein expression. The relative density is shown in histograms. Data are from 3 independent tests (n=6 per group). SAE, sepsis associated encephalopathy; PRB, probenecid; HE, hematoxylin and eosin; AMPK, adenosine monophosphate-activated protein kinase; GAPDH, glyceraldehyde 3-phosphate dehydrogenase.

the treatment of SAE. Pyroptosis and autophagy are common in a variety of diseases, such as sepsis, cancer, and trauma. Several research studies have examined the relationship between pyroptosis and autophagy (42,43). Indeed, our present study showed that autophagy and pyroptosis are involved in the occurrence of SAE in mice, and autophagy may inhibit the occurrence of pyroptosis. Protecting tissues and cells from pyroptosis may provide a novel avenue for sepsis treatment and warrants further research. In addition, further studies should be conducted to investigate the regulatory relationship between pyroptosis and autophagy.

Conclusions

The present findings in this investigation demonstrated an important role of pannexin-1 in SAE. Indeed, pannexin-1 can regulate pyroptosis through autophagy, which is associated with the AMPK signaling pathway. This study suggested an essential role for the interaction between

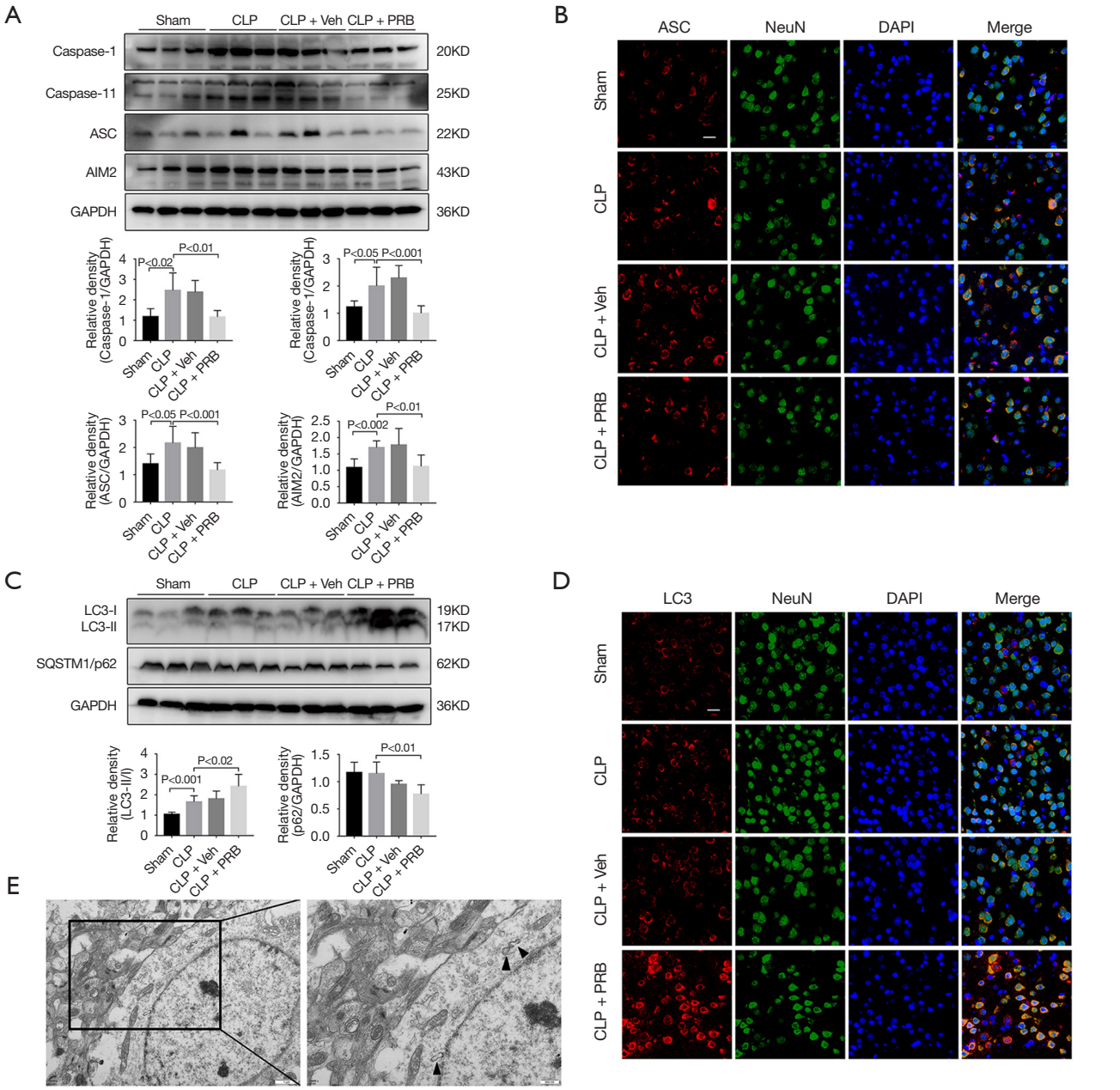

Figure 5 Pyroptosis was alleviated and autophagy was effectively activated in SAE mice after treatment with PRB. (A) Protein expression of caspase-1, caspase-11, ASC, and AIM2 were detected by Western blotting (12 hours after surgery). The protein levels were normalized to GAPDH and are shown as relative arbitrary units in the histograms. (B) The fluorescence intensities of ASC (red) and NeuN (green) were detected by immunofluorescence staining (12 hours after surgery). Scale bar =20 μm. (C) The levels of LC3-II/I and p62 protein expression were detected by Western blotting (12 hours post operation). GAPDH was used as internal reference for normalization and the results are shown as relative protein levels in the histograms. (D) The fluorescence intensities of LC3 (red) and NeuN (green) were detected by immunofluorescence staining (12 hours after surgery). Scale bar =20 μm. (E) At 12 hours after surgery, the ultrastructure of the cortical neurons in the CLP + PRB group observed by TEM revealed that the organelle structure as generally normal and the substances in autophagosomes were effectively degraded and formed multiple autophagy vesicles. Scale bar =1 and 2 μm. Data are from 3 independent tests (n=6 per group). SAE, sepsis associated encephalopathy; PRB, probenecid; GAPDH, glyceraldehyde 3-phosphate dehydrogenase; TEM, transmission electron microscope.

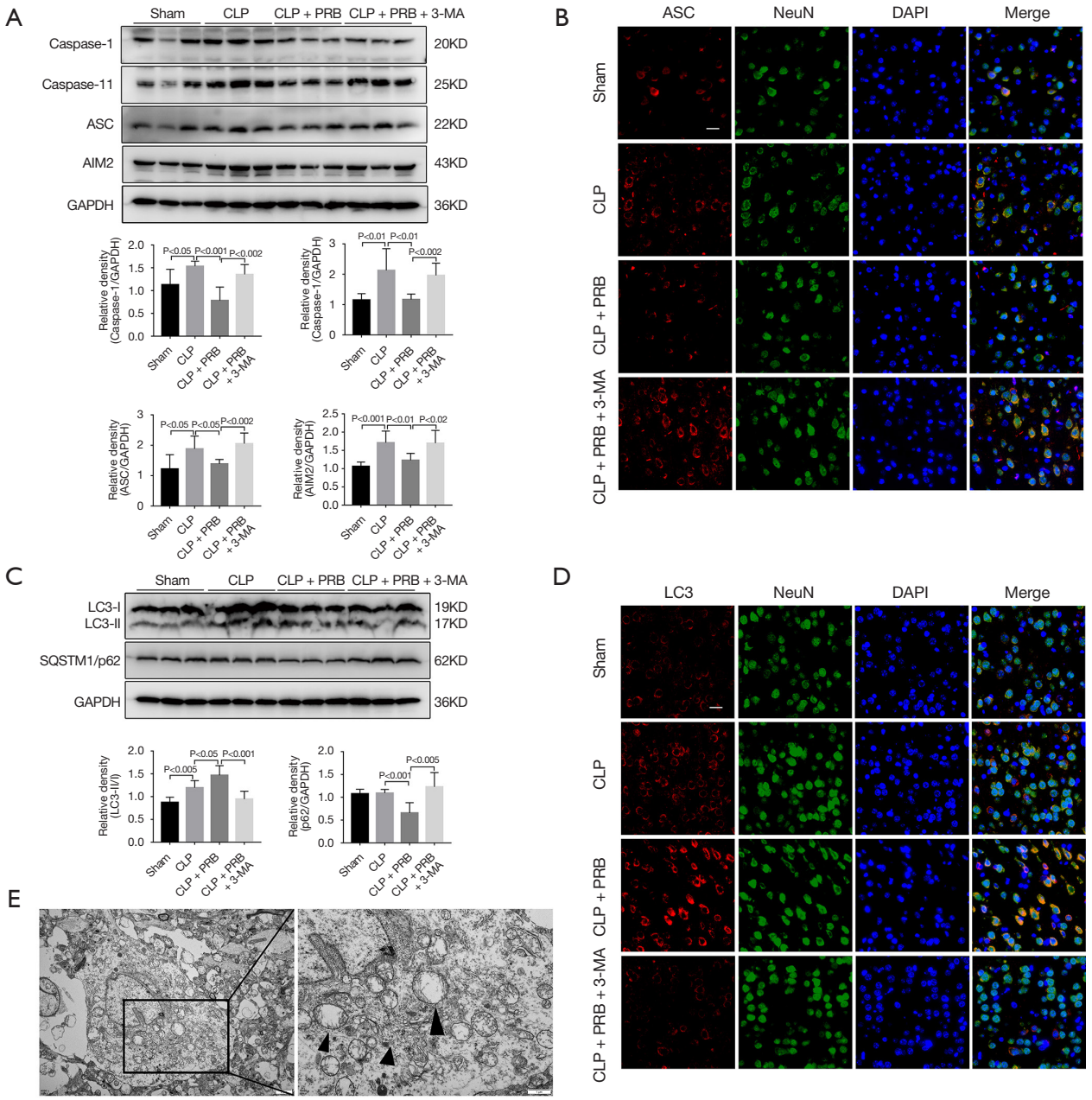

Figure 6 Administration of 3-MA in the CLP + PRB group inhibited neuron autophagy and activated pyroptosis. (A) Protein expression of caspase-1, caspase-11, ASC, and AIM2 were detected by Western blotting (12 hours post operation). GAPDH was used as internal reference for normalization and the results are shown as relative protein levels in the histograms. (B) The fluorescence intensities of ASC (red) and NeuN (green) were detected by immunofluorescence staining (12 hours after surgery). Scale bar =20 μm. (C) Protein expression of LC3II/I and p62 were detected by Western blotting (12 hours after surgery). The protein levels were normalized to GAPDH and are shown as relative arbitrary units in the histograms. (D) The fluorescence intensities of LC3 (red) and NeuN (green) were detected by immunofluorescence staining (12 hours after surgery). Scale bar =20 μm. (E) At 12 hours after surgery, the ultrastructure of the cortical neurons in CLP + PRB + C-MA group was observed by TEM. There was no autophagosome formation in the cortical neurons but obvious mitochondrial swelling and mitochondrial crest rupture were observed. Scale bar =1 and 2 μm. Three independent tests were conducted to acquire the data (n=6 per group). SAE, sepsis associated encephalopathy; PRB, probenecid; ASC, apoptosis-associated speck-like protein; AIM2, absent in melanoma 2; GAPDH, glyceraldehyde 3-phosphate dehydrogenase; TEM, transmission electron microscope.

pannexin-1, pyroptosis, and autophagy in SAE progression and provided preliminary data regarding the protective effects of pannexin-1 antagonists in SAE.

Acknowledgments

Funding: This work was supported by grants from the National Science Foundation of China (81630038, 81971433, 81971428, 81771634, 81842011, 81330016, 81801629, 82071353); the National Key R&D Program of China (2017YFA0104200, 2017YFA0104201); the Ministry of Education of China (IRT0935); the Fundamental Research Funds for the Central Universities (SCU2020D006); the Science and Technology Bureau of Sichuan Province (2021YFS0029, 2020YFS0041, 2016TD0002); and the Clinical Discipline Program (Neonatology) from the Ministry of Health of China (1311200003303).

Footnote

Reporting Checklist: The authors have completed the ARRIVE reporting checklist. Available at https://dx.doi.org/10.21037/atm-21-6579

Data Sharing Statement: Available at https://dx.doi.org/10.21037/atm-21-6579

Conflicts of Interest: All authors have completed the ICMJE uniform disclosure form (available at https://dx.doi.org/10.21037/atm-21-6579). The authors report funding from the National Science Foundation of China (81630038, 81971433, 81971428, 81771634, 81842011, 81330016, 81801629, 82071353), the National Key R&D Program of China (2017YFA0104200, 2017YFA0104201), the Ministry of Education of China (IRT0935), the Fundamental Research Funds for the Central Universities (SCU2020D006), the Science and Technology Bureau of Sichuan Province (2021YFS0029, 2020YFS0041, 2016TD0002), and the Clinical Discipline Program (Neonatology) from the Ministry of Health of China (1311200003303). The authors have no other conflicts of interest to declare.

Ethical Statement: The authors are accountable for all aspects of the work in ensuring that questions related to the accuracy or integrity of any part of the work are appropriately investigated and resolved. All animal experiments were approved by the Research Animal Care Committee of the Sichuan University (Sichuan, China) [No. (2021) Animal Ethics Approval No. 046], in compliance with Sichuan University guidelines for the care and use of animals.

References

1. Tiru B, DiNino EK, Orenstein A, et al. The Economic and Humanistic Burden of Severe Sepsis. Pharmacoeconomics 2015;33:925-37.
2. Rudd KE, Johnson SC, Agesa KM, et al. Global, regional, and national sepsis incidence and mortality, 1990-2017: analysis for the Global Burden of Disease Study. Lancet 2020;395:200-11.
3. Kolaczkowska E, Kubes P. Neutrophil recruitment and function in health and inflammation. Nat Rev Immunol 2013;13:159-75.
4. Cecconi M, Evans L, Levy M, et al. Sepsis and septic shock. Lancet 2018;392:75-87.
5. Singer M, Deutschman CS, Seymour CW, et al. The Third International Consensus Definitions for Sepsis and Septic Shock (Sepsis-3). JAMA 2016;315:801-10.
6. Young GB, Bolton CF, Austin TW, et al. The encephalopathy associated with septic illness. Clin Invest Med 1990;13:297-304.
7. Chaudhry N, Duggal AK. Sepsis Associated Encephalopathy. Adv Med 2014;2014:762320.
8. Molnár L, Fülesdi B, Németh N, et al. Sepsis-associated encephalopathy: A review of literature. Neurol India 2018;66:352-61.
9. Ehler J, Petzold A, Wittstock M, et al. The prognostic value of neurofilament levels in patients with sepsis-associated encephalopathy - A prospective, pilot observational study. PLoS One 2019;14:e0211184.
10. D'Arcy MS. Cell death: a review of the major forms of apoptosis, necrosis and autophagy. Cell Biol Int 2019;43:582-92.
11. Shalini S, Dorstyn L, Dawar S, et al. Old, new and

emerging functions of caspases. Cell Death Differ 2015;22:526-39.
12. Shi J, Gao W, Shao F. Pyroptosis: Gasdermin-Mediated Programmed Necrotic Cell Death. Trends Biochem Sci 2017;42:245-54.
13. Chen X, He WT, Hu L, et al. Pyroptosis is driven by non-selective gasdermin-D pore and its morphology is different from MLKL channel-mediated necroptosis. Cell Res 2016;26:1007-20.
14. Dong T, Liao D, Liu X, et al. Using Small Molecules to Dissect Non-apoptotic Programmed Cell Death: Necroptosis, Ferroptosis, and Pyroptosis. Chembiochem 2015;16:2557-61.
15. Eskelinen EL. Maturation of autophagic vacuoles in Mammalian cells. Autophagy 2005;1:1-10.
16. Galluzzi L, Green DR. Autophagy-Independent Functions of the Autophagy Machinery. Cell 2019;177:1682-99.
17. Pelegrin P, Surprenant A. Pannexin-1 mediates large pore formation and interleukin-1beta release by the ATP-gated P2X7 receptor. EMBO J 2006;25:5071-82.
18. Yang D, He Y, Muñoz-Planillo R, et al. Caspase-11 Requires the Pannexin-1 Channel and the Purinergic P2X7 Pore to Mediate Pyroptosis and Endotoxic Shock. Immunity 2015;43:923-32.
19. Robbins N, Koch SE, Tranter M, et al. The history and future of probenecid. Cardiovasc Toxicol 2012;12:1-9.
20. Silverman W, Locovei S, Dahl G. Probenecid, a gout remedy, inhibits pannexin 1 channels. Am J Physiol Cell Physiol 2008;295:C761-7.
21. Silverman WR, de Rivero Vaccari JP, Locovei S, et al. The pannexin 1 channel activates the inflammasome in neurons and astrocytes. J Biol Chem 2009;284:18143-51.
22. Wu YT, Tan HL, Shui G, et al. Dual role of 3-methyladenine in modulation of autophagy via different temporal patterns of inhibition on class I and III phosphoinositide 3-kinase. J Biol Chem 2010;285:10850-61.
23. Egan DF, Shackelford DB, Mihaylova MM, et al. Phosphorylation of ULK1 (hATG1) by AMP-activated protein kinase connects energy sensing to mitophagy. Science 2011;331:456-61.
24. Zhang D, Wang W, Sun X, et al. AMPK regulates autophagy by phosphorylating BECN1 at threonine 388. Autophagy 2016;12:1447-59.
25. Chen KW, Groß CJ, Sotomayor FV, et al. The neutrophil NLRC4 inflammasome selectively promotes IL-1β maturation without pyroptosis during acute Salmonella challenge. Cell Rep 2014;8:570-82.
26. Broz P. Immunology: Caspase target drives pyroptosis. Nature 2015;526:642-3.
27. Jiang P, Mizushima N. LC3- and p62-based biochemical methods for the analysis of autophagy progression in mammalian cells. Methods 2015;75:13-8.
28. Johansen T, Lamark T. Selective autophagy mediated by autophagic adapter proteins. Autophagy 2011;7:279-96.
29. Rogov V, Dötsch V, Johansen T, et al. Interactions between autophagy receptors and ubiquitin-like proteins form the molecular basis for selective autophagy. Mol Cell 2014;53:167-78.
30. Rittirsch D, Huber-Lang MS, Flierl MA, et al. Immunodesign of experimental sepsis by cecal ligation and puncture. Nat Protoc 2009;4:31-6.
31. Burma NE, Bonin RP, Leduc-Pessah H, et al. Blocking microglial pannexin-1 channels alleviates morphine withdrawal in rodents. Nat Med 2017;23:355-60.
32. Zhang Z, Lei Y, Yan C, et al. Probenecid Relieves Cerebral Dysfunction of Sepsis by Inhibiting Pannexin 1-Dependent ATP Release. Inflammation 2019;42:1082-92.
33. Zhang X, Yan H, Yuan Y, et al. Cerebral ischemia-reperfusion-induced autophagy protects against neuronal injury by mitochondrial clearance. Autophagy 2013;9:1321-33.
34. He Q, Li Z, Wang Y, et al. Resveratrol alleviates cerebral ischemia/reperfusion injury in rats by inhibiting NLRP3 inflammasome activation through Sirt1-dependent autophagy induction. Int Immunopharmacol 2017;50:208-15.
35. Kafa IM, Uysal M, Bakirci S, et al. Sepsis induces apoptotic cell death in different regions of the brain in a rat model of sepsis. Acta Neurobiol Exp (Wars) 2010;70:246-60.
36. Bauernfeind FG, Horvath G, Stutz A, et al. Cutting edge: NF-kappaB activating pattern recognition and cytokine receptors license NLRP3 inflammasome activation by regulating NLRP3 expression. J Immunol 2009;183:787-91.
37. Schroder K, Tschopp J. The inflammasomes. Cell 2010;140:821-32.
38. Liu L, Sun B. Neutrophil pyroptosis: new perspectives on sepsis. Cell Mol Life Sci 2019;76:2031-42.
39. Kabeya Y, Mizushima N, Ueno T, et al. LC3, a mammalian homologue of yeast Apg8p, is localized in autophagosome membranes after processing. EMBO J 2000;19:5720-8.
40. Komatsu M, Waguri S, Koike M, et al. Homeostatic levels of p62 control cytoplasmic inclusion body formation in autophagy-deficient mice. Cell 2007;131:1149-63.
41. Kageyama S, Gudmundsson SR, Sou YS, et al. p62/

SQSTM1-droplet serves as a platform for autophagosome formation and anti-oxidative stress response. Nat Commun 2021;12:16.
42. Li MY, Zhu XL, Zhao BX, et al. Adrenomedullin alleviates the pyroptosis of Leydig cells by promoting autophagy via the ROS-AMPK-mTOR axis. Cell Death Dis 2019;10:489.
43. Gao C, Yan Y, Chen G, et al. Autophagy Activation Represses Pyroptosis through the IL-13 and JAK1/STAT1 Pathways in a Mouse Model of Moderate Traumatic Brain Injury. ACS Chem Neurosci 2020;11:4231-9.

(English Language Editor: J. Teoh)

Cite this article as: Lei Y, Zhou R, Sun X, Tang F, Gao H, Chen L, Li X. The pannexin-1 channel regulates pyroptosis through autophagy in a mouse model of sepsis-associated encephalopathy. Ann Transl Med 2021;9(24):1802. doi: 10.21037/atm-21-6579

